BNL-222179-2021-TECH
EIC-ADD-TN-022

ESR Magnet vibrational specifications for dynamic orbit stability at the IP

B. Podobedov

September 2021

Electron-Ion Collider

Brookhaven National Laboratory

U.S. Department of Energy

USDOE Office of Science (SC), Nuclear Physics (NP) (SC-26)

DISCLAIMER

ESR Magnet Vibrational Specifications for Dynamic Orbit Stability at the IP

Boris Podobedov and Daniel Marx

September 1 , 2021

1. Introduction

In this study the effects of magnet vibrations (quadrupole displacements and dipole rolls) on the electron beam orbit stability at the interaction points (IPs) of the EIC [1] have been quantified. Maintaining positional orbit offsets at the IP within a small fraction of the respective beam size in both planes is important for achieving the design luminosity due to beam-beam effects. Specifying exact tolerances for the residual orbit jitter at the IP requires detailed beam-beam simulations not available to-date. To get some preliminary estimates here we use a simplified and easily scalable criterion that the integrated beam motion must be restricted to 10% of the rms beam size at the IP. The motivation for this comes from experience at RHIC. RHIC beams have a horizontal jitter amplitude of approximately 10% of the rms beam size at a frequency of around 10 Hz, which is driven by vibrations of the IR triplet quads induced by helium flow [2]. The 10 Hz IR-orbit feedback system, which corrects both position and angle, showed no discernible effect on emittance growth [3]. We therefore make the assumption that a 10% rms jitter of the electron beam should cause a tolerable effect on the hadron beam.

The orbit motion frequencies we consider are from a fraction of a Hz to roughly 100 Hz. Large-amplitude magnet vibrations at higher frequencies are not expected. Slower motions (long term drifts) and their implications will be addressed in separate studies

For simulations reported in this note we used the 18 GeV ESR 2-IP lattice version 5.3. While the lattice is constantly evolving, the changes are not expected to affect the findings of this note, as they primarily rely on the linear lattice properties.

The rest of this note is organized as follows. In Section 2 we describe the amplification factors relating quadrupole displacements to orbit offsets at the IP. In Section 3 we present the floor vibration model we adopted by approximating earlier measurements performed by others at RHIC and elsewhere. Section 4 contains estimates of the orbit motion at the IP due to vibrating quadrupoles, ignoring possible resonant amplification due to girders. Section 5 contains estimates of orbit jitter due to vibrating dipole rolls. In Section 6 we consider resonant amplification of magnet motion due to girders and describe the range of acceptable girder resonance frequencies. Finally, in Section 7, we summarize the results and outline some future work.

2. Amplification factors for displaced quadrupoles

We define the quadrupole-to-IP closed-orbit amplification factors as follows. For the horizontal plane, assume a random uncorrelated displacement, δ_x, of each magnet within a quadrupole family or multiple families, which follows a Gaussian distribution. The expected rms resulting closed orbit deviation ΔX at the IP location ($s = s_{IP}$), normalized to the rms quadrupole displacement, $\langle \delta_x \rangle_{\mathrm{rms}}$, gives the amplification factor,

$$AF_{x,x} = \langle \Delta X(s_{IP}) \rangle_{\mathrm{rms}} / \langle \delta_x \rangle_{\mathrm{rms}}. \tag{2.1}$$

In general, four amplification factors must be considered: from horizontal quadrupole displacements to the horizontal orbit at the IP, given by Eq. (2.1), a similar quantity for the vertical, $AF_{y,y}$, and the cross-terms, $AF_{x,y}$ and $AF_{y,x}$. For some quadrupoles located in the coupled sections within the solenoid spin rotators, the cross-terms could be significant.

Summing the contributions from N individual magnets, $i = 1,2,\dots,N,$ the amplification factors could be estimated from the closed-orbit formula due to the dipole kick θ by the offset quadrupole,

$$\langle X(s_{IP})\rangle_{\mathrm{rms}}, = \sqrt{\beta_x^{IP}}\frac{\sqrt{N\langle\beta_x(s_i)\rangle}}{2\sqrt{2}\sin(\pi Q_x)}\langle\theta_{x,i}\rangle_{\mathrm{rms}}, \tag{2.2}$$

$$\theta_{x,i} = (Kl)_i\delta_{x,i}, \tag{2.3}$$

where $1/(Kl)_i$ and s_i are the focal lengths and longitudinal positions of the magnets respectively and the worst phase advance is assumed for simplicity. Similar expressions apply in the vertical plane.

This calculation is easy for a single quad family, especially when all magnets have the same betatron functions and betatron phases. However, it becomes tedious (more terms) or less precise (with some approximate averaging) if the magnets have a significant spread in lattice function values. Therefore, we opted to calculate the amplification factors with Elegant [4] and MAD-X [5]. We also checked that the results agree with equations above for some tractable subsets of cases.

Calculations were performed as follows. Quadrupoles within a family (or a set of families) were randomly displaced with $1\ \mu\mathrm{m}$ rms in x or y, and then the resulting closed orbit was calculated for both planes, see the examples in Fig. 1 for the vertical. This was repeated 300 times to get enough statistics. The rms of these closed orbit values at each of the IPs were calculated separately, then averaged together, and, finally, normalized to the original $1\ \mu\mathrm{m}$ rms quadrupole displacement. The resulting amplification factors for selected groups of quadrupoles are listed in Table 1.

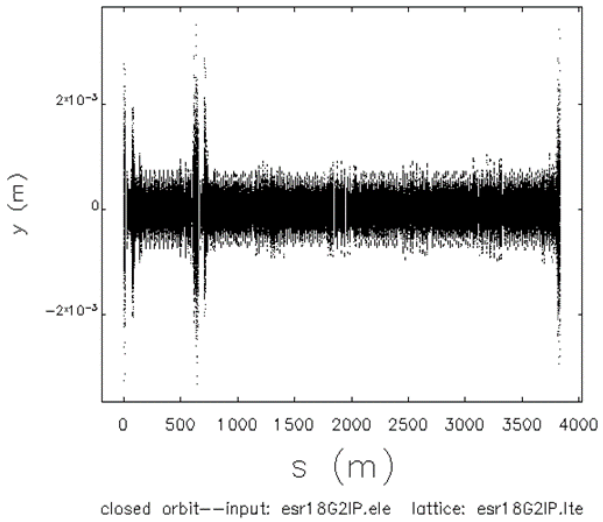

Figure 1: Three hundred super-imposed vertical closed orbits due to random vertical displacements of all quads with $\langle \delta_y \rangle_{rms}$= 1 μm. IPs are located at s=0 and s=641 m.

Group: names (count)	$AF_{x,x}$	$AF_{y,y}$	$AF_{x,y}$	$AF_{y,x}$
All: * (532)	13	9.1	1.2	5.9
"IR": E* (58)	8.4	5.0	<<1	<<1
"Solenoid": HQ[A,B]* (52)	6.4	6.7	1.2	6.1
"Normal": (the rest) (422)	7.1	3.4	<<1	<<1

Table 1: Amplification factors for selected groups of quadrupoles from Elegant calculations.

Very close values for the amplification factors were independently obtained in MAD-X calculations.

3. Ground vibration amplitude and coherence

To calculate the orbit jitter at the IP due to vibrating quadrupoles or other accelerator components we need to know the amplitude of the vibrations. Disregarding other possible sources which may cause magnet vibration, e. g. cooling water or helium flow, here we only consider the ground (floor) vibrations.

In 2006 H. Ehrlichmann et al. took measurements of ground vibration in the RHIC tunnel at two locations: building 1005 and Phenix (IP8). The results are available from DESY's database of ground motion measurements at accelerator facilities worldwide [6]. We have access to all these data, both raw and Power Spectral Density (PSD) in 15-minute intervals. For the purposes of this note we simply averaged the IP8 vertical measurements over all these intervals to obtain the mean PSD, denoted $\overline{P_0}$ below, which is plotted in Fig. 2. (The horizontal PSD is somewhat smaller, and, due to flat beams, less critical. Here we will simply assume that the same vibrational spectrum applies in both planes. This could be revisited later). This PSD drops sharply with frequency and, especially at lower frequencies, agrees well with ~$1/f^4$ scaling, expected from theory [7]. At higher frequencies there is also a significant amount of cultural noise, including some sharp peaks, e.g. in the vicinity of 5, 8, 15, 30 and 60 Hz.

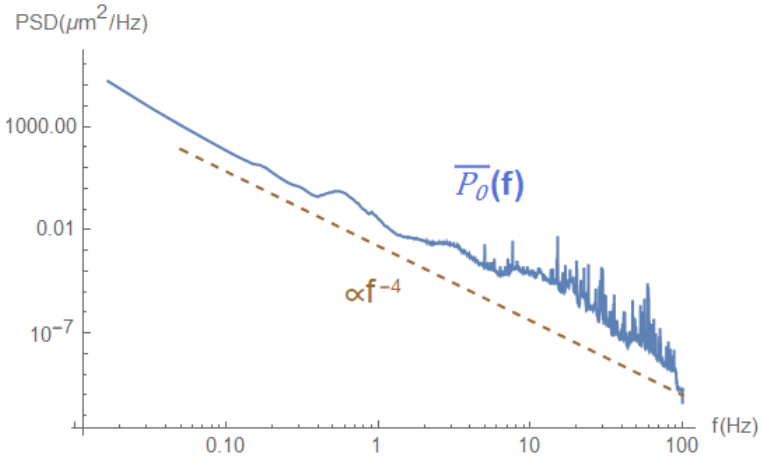

Figure 2: Average PSD for floor vibrations in RHIC tunnel from 2006 measurements and ~1/f⁴ scaling

We also compared the RHIC measurements with those from the NSLS-II experimental floor [8] and found reasonable agreement. NSLS-II floor measurements exhibit a clear day-night variation cycle and typically measure from 15 to 60 nm rms in the horizontal and 20 to 100 nm rms in the vertical in the bandwidth of 2-100 Hz. The averaged data from RHIC we are using (Fig. 2) results in 70 nm rms in the same bandwidth.

Ground motion divergence at low frequency does not present a serious stability problem for an accelerator, because, as the frequency gets lower, the wavelength of ground vibrations increases, and larger and larger fractions of the entire accelerator essentially move together. This is usually described by introducing the concept of ground-motion coherence, which defines the spectral content of correlated motion between two different locations. Mathematically it is defined as the ratio of the cross-spectral density (Fourier transform pair of the cross-correlation function), $P_{z_1,\,z_2}(\omega)$, between the motions at two locations normalized to their individual PSDs,

$$C_{z_1 z_2}(\omega) = \frac{|P_{z_1,\,z_2}(\omega)|^2}{PSD_{z_1}(\omega) PSD_{z_2}(\omega)}. \tag{3.1}$$

Ground motion coherence can be measured (with the mathematical quantities in (3.1) replaced with the measured ones which include signal windowing, averaging, and filtering in time and frequency domains), but it obviously requires simultaneous measurements performed at a minimum of two locations. To our knowledge such measurements have never been performed at RHIC. However, they have been performed at many other facilities, in particular, at NSLS-II [8, 9], LHC [10], and APS [11]. While the details vary significantly (between the labs, between locations on the same site, as well as with time at the same location), as is pointed out in [9-11], ground motion becomes mostly coherent at frequencies below 1 Hz and gradually loses coherence at higher frequencies, on the order of 10 Hz. In the spatial domain, these 1 Hz and 10 Hz frequencies correspond to the coherence lengths on the order of 100 m and below 10 m respectively (see e.g. Figs. 8, 11 in [8] and Fig. 4 in [11]).

Lacking ground motion coherence measurements at RHIC we adopted the following model here. We assume that for the length-scales relevant to the EIC (betatron wavelength ~100 m), the ground motion is fully coherent below 1 Hz and fully incoherent above 10 Hz (exact value of this upper frequency is not critical), with some gradual ramp-down in the intermediate region. Because we only need to consider the effect of the incoherent motion we ignore the effect of frequencies below 1 Hz, and fully account for those above 10 Hz. In the intermediate region we linearly ramp-up the incoherent motion PSD fraction from 0 to 1. This gradual ramp-up is qualitatively consistent with a much more detailed measurement-based model from APS [11].

Specifically, to define the relevant floor vibration PSD with the coherence effects approximately included, we multiply the PSD from Fig. 2 by the function

$$\kappa(f) = \begin{cases} 0, & f < f_1 \\ \frac{f-f_1}{f_2-f_1}, & f_1 \le f \le f_2 \\ 1, & f > f_2 \end{cases}, \tag{3.2}$$

with f_2=1 Hz and f_2=10 Hz.

Together with the original PSD from Fig. 2 this scaled PSD is plotted in Fig. 3. Integrated rms totals for both are shown in the legend.

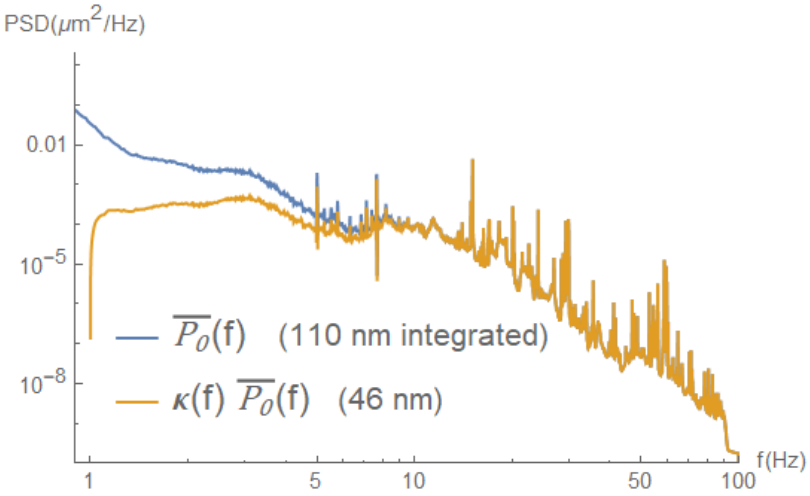

Figure 3: Original ground vibration PSD from Fig. 2 and the one scaled to account for the ground motion coherence. Integrated rms totals are shown for the bandwidth of 1-100 Hz.

4. Implications for ESR

Let's assume that the floor vibrations quantified above are directly transferred to the quadrupoles. For simplicity we ignore the screening effects of the vacuum chamber due to eddy currents, which makes our estimate more conservative. The induced rms orbit noise at the IP can now be estimated by

multiplying the scaled PSD from Fig. 3 by the amplification factors given in Table 1, and integrating over frequency. Calculating the effect from all quadrupole magnets (i.e. taking the numbers from the first row of the table), and assuming uncorrelated horizontal and vertical vibrations, we get for the orbit motion at the IP

$$\begin{aligned} \langle \delta_x \rangle_{\mathrm{rms}} &= 660 \text{ nm} \\ \langle \delta_y \rangle_{\mathrm{rms}} &= 420 \text{ nm}\,' \end{aligned} \tag{4.1}$$

These make approximately 0.6% and 4% of the corresponding rms beam sizes, which is below our nominal 10% goal. (CDR Table 3.3 lists for the ESR at 18 GeV $\sigma_x^{IP} = 119\ \mu m$ and $\sigma_y^{IP} = 11\ \mu m$.)

However, the number in the vertical plane is not entirely negligible. Considering the many approximations made along the way, and the fact that we are only considering one of the factors potentially contributing to the orbit jitter at the IP, it would be prudent to plan for a local orbit feedback system to stabilize the motion further.

5. Dipole rolls

Another type of magnet vibrations that could increase the orbit jitter are dipole rolls. If a dipole is rotated with respect to the beam axis by angle θ, the nominally vertical magnetic field $\bar{B} = B_0\{0, 1\}$ acquires a horizontal component, $\bar{B} = B_0\{sin(\theta),\ cos(\theta)\}$, which results in a vertical beam kick. For small θ, the change in the horizontal kick could be neglected.

This effect was simulated in Elegant and MAD-X by setting a random roll angle to all dipoles in the lattice and calculating the corresponding orbit shift at the IPs. An example is shown in Fig. 4, which illustrates that dipole rolls with $\langle \theta \rangle_{rms} = 100$ μrad result in an IP rms orbit jitter of about 33 μm. Simulations with a 3 urad orbit roll gave the required 1 um IP rms orbit jitter. A close value was also obtained analytically.

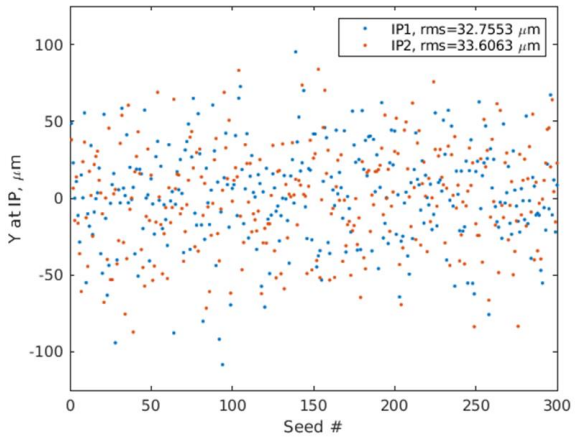

Figure 4: Vertical orbit offsets at IPs due to 100 μrad rms dipole rolls. Legend shows the resulting orbit rms over 300 seed samples at the IPs.

Achieving dipole roll jitter of 3 μrad rms does not appear challenging. For instance, assume that the roll is mainly driven by differential floor vibrations between four anchor points holding the magnet which are spread apart transversely by a distance on the order of one meter. Taking the uncorrelated vertical rms motions of 100 nm rms (see Fig. 3), we estimate the rms magnet roll of order of 100 nrad. Moreover, dynamic roll specifications for dipoles on the micro-radian level have been achieved at light sources.

6. Girder amplification

So far, we have not considered the effect of magnet girders. They are known to resonantly amplify floor vibrations at certain frequencies corresponding to the mechanical resonances of the structure (girder loaded with magnets). Due to the rapid falloff of the ground vibration spectral power with frequency, it is desirable to design girders with higher resonance frequencies, so that the total added effect due to girder amplification is small.

Typical accelerator girder structures may have many (n>>1) prominent resonant modes, differing in spatial shape (e.g. "rocking", "twisting", etc.), each with its own resonant frequency $\omega_{0,n}$ and quality factor Q_n. Typical resonant frequencies are in tens of Hz, while the damping factors, $\xi_n = \frac{1}{2Q_n}$, are in the range of [0.01-0.04].

Here we take a simplified approach to the problem by modelling the girder as a 1D harmonic oscillator with the natural frequency ω_0 and the damping factor ξ. The oscillator is driven at frequency ω by moving the anchor point x_a, as shown in Fig. 5, and the damping force is proportional to $\dot{x}_m(t)$.

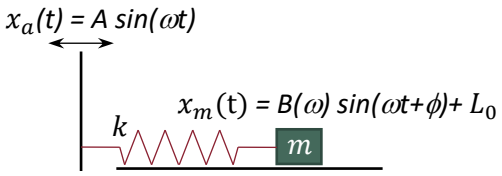

Figure 5: Harmonic oscillator model of a girder driven by floor vibrations. Here k and L_0 denote the spring constant and its unstretched length.

The equation of motion can be written as

$$\ddot{x}_m + 2\xi\omega_0\dot{x}_m + {\omega_0}^2 x_m = {\omega_0}^2(x_a(t) + L_0), \tag{6.1}$$

where $\omega_0 = \sqrt{k/m}$. For $x_a(t) = A\ sin\omega t$, it is equivalent to the classical problem of a harmonically driven oscillator. The amplitude of the steady-state solution, $x_m(t) = B(\omega)\sin(\omega\, t + \phi) + L_0$, is given by the well-known resonance expression

$$|B(\omega)| = \frac{|A|}{\sqrt{(1-(\omega/\omega_0)^2)^2+4\xi^2(\omega/\omega_0)^2}}, \tag{6.2}$$

which reaches its maximum

$$|B(\omega)|_{max} = \frac{|A|}{2\xi\sqrt{1-\xi^2}} = \frac{2Q^2|A|}{\sqrt{4Q^2-1}} \tag{6.3}$$

at the resonant frequency

$$\omega_{res} = \omega_0\sqrt{1-2\,\xi^2} \approx \omega_0. \tag{6.4}$$

The approximate equality above assumes the practically relevant case of $\xi \ll 1$.

Alternatively, we can solve (6.1) for the amplitude $C(\omega)$ of the relative motion of the mass to the anchor point (i.e. the girder with respect to the floor). Re-writing (6.1) in terms of $z_m(t) = x_m(t) - x_a(t) - L_0$ and assuming a steady-state solution of $z_m(t) = C(\omega)\sin(\omega t + \varphi)$ results in the amplitude amplification factor from x_a to z_m

$$|C(\omega)/A| = \sqrt{\frac{1+4\xi^2(\omega/\omega_0)^2}{(1-(\omega/\omega_0)^2)^2+4\xi^2(\omega/\omega_0)^2}}, \tag{6.5}$$

which is equivalent to (6.2) for the case of small ξ. Similar to the previous case, near the resonant frequency,

$$\omega_{res} = \omega_0\frac{\sqrt{\sqrt{1+8\,\xi^2}-1}}{2\xi} \approx \omega_0, \tag{6.6}$$

the amplitude amplification can become quite large,

$$|C(\omega)/A|_{max} \approx \frac{1}{2\xi} = Q. \tag{6.7}$$

The amplitude amplification factor is sometimes referred as transmissibility (or the absolute value of complex transmissibility). When squared, this factor gives the amplification factor for the power spectral density. For sinusoidally varying $x_a(t)$, as considered above, this fact is trivial. For the general excitation function $x_a(t)$ this is easily confirmed by Fourier transforming (6.1) to express $\tilde{z}_m(\omega)$ in terms of $\tilde{x}_a(\omega)$, and then making use of the power spectral density definition (e.g. [12]), $PSD_{u(t)}(\omega) = \lim_{T\to\infty}\frac{1}{T}|\tilde{u}_T(\omega)|^2$, where $u_T(t) = u(t)$ for $0 < t < T$ and zero otherwise.

Specifically, taking $x_a(t)$ and $z_m(t)$ as the input and output of the system, we can write for the spectral power amplification,

$$G(\omega, \omega_0, \xi\,) = \frac{PSD_{z_m}(\omega)}{PSD_{x_a}(\omega)} = \frac{1+4\,\xi^2(\omega/\omega_0)^2}{(1-(\omega/\omega_0)^2)^2+4\,\xi^2(\omega/\omega_0)^2}. \tag{6.8}$$

Multiplying this by the scaled PSD $\kappa(\omega)\overline{P_0}(\omega)$ from Fig. 3, we can now include the effect of the girder resonances. This is illustrated in Fig. 6 for $\mathrm{f}_{res} = \omega_0/(2\pi)$=10 Hz. (Note the change in subscript. Here and below f_{res} stands for the natural (undamped) resonant frequency of the girder $\omega_0/(2\pi)$.)

For the two values of the damping coefficient shown in the figure, the girder resonance amplifies the integrated ground motion by factors of 5.6 and 4.0. Such amplification would obviously be undesirable for orbit stability, so girders must be designed with higher resonant frequencies.

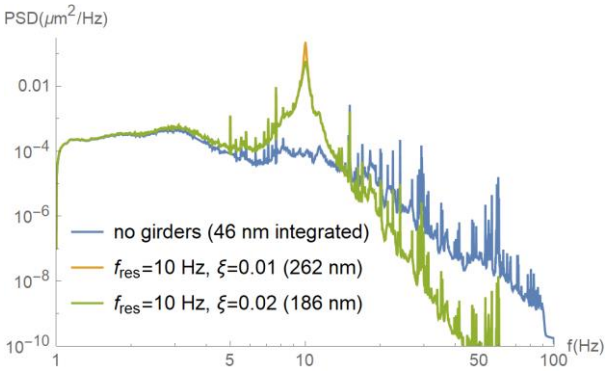

Figure 6: Vibration PSD including the resonant girder amplification. Resonance parameters are shown in the legend.

To investigate this further we define the girder amplification factor as

$$AF_g(\omega_0,\xi) = \frac{\int G(\omega,\omega_0,\xi)\kappa(\omega)\overline{P_0}(\omega)d\omega}{\int \kappa(\omega)\overline{P_0}(\omega)d\omega}, \tag{6.9}$$

where $\kappa(\omega)$ was defined in (3.2).

We now plot this factor as a function of the resonant frequency in Fig. 7.

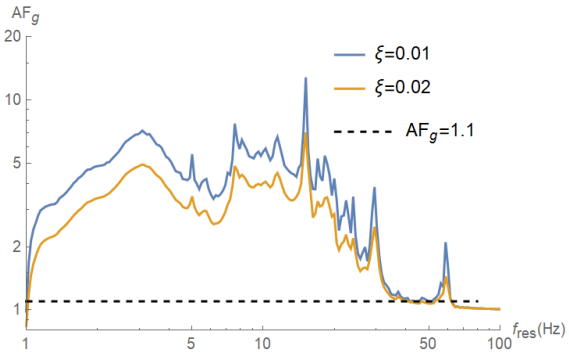

Figure 7: Girder amplification factor vs. resonance frequency.

The figure illustrates that if one requires the girder resonances to amplify the floor vibrations by no more than 10% then the girder resonant frequency must exceed 40 Hz, and the vibrational peaks near 60 Hz should also be avoided. Due to rapid falloff of the amplification factor after the 30 Hz peak, this

minimum resonant frequency value (40 Hz) is not too sensitive to some relaxation of the maximum allowed amplification requirement. Similarly, if a stronger resonant damping is achieved, the resonant frequency could be chosen somewhat lower, but the ξ-dependence in this frequency region is rather weak.

7. Summary

Vibrational specifications for the quadrupole displacements and dipole rolls were analyzed for their effect on the ESR orbit motion at the IPs. This was done by means of Elegant and MAD-X simulations and cross-checked with analytical calculations, wherever possible.

The magnet motion was assumed to be driven by ground vibrations only. A ground vibration model was developed based on RHIC IP8 measurements performed in 2006. It was found to be in good agreement with the typical vibration levels on the NSLS-II experimental floor during the noisier parts of the 24-hour cycle. As expected, the vibration PSD diverges at low frequencies, however, vibrations at these frequencies play a progressively smaller role due to accelerator components moving in phase with each other. Lacking RHIC tunnel ground coherence measurements, we adopted an approximate model to describe this effect by assuming fully coherent ground motion below 1 Hz and fully incoherent motion above 10 Hz, with a smooth transition in between.

Considering only the quadrupole vibrations driven by ground motion, we showed that within this model the expected rms orbit variation at the IPs is about 4% of σ_y at the IP. This number is below the nominal 10% of σ_y goal, but the margin is not very large. Due to approximations made in the model as well as other potential contributions neglected, this suggests that a local orbit feedback to stabilize the beam size at the IP could be useful. Feedback design will be considered separately; however, it does not appear to be challenging. Of course, this assumes that other accelerator components are carefully designed so that they do not cause significant orbit perturbations, especially at higher frequencies.

Due to the much larger beam size in the horizontal plane, the expected effect from the quadrupole vibrations is predicted to be much lower, at less than 1% of the beam size, which is not expected to cause any issues. In addition, the effect of dipole rolls was analyzed and shown to be manageable, as long as the rolls are kept sufficiently below 3 μrad rms, which is considered readily achievable.

Finally, the effect of girder resonances was analyzed using a simple damped harmonic-oscillator model. This preliminary analysis shows that the lowest girder resonant frequency should exceed 40 Hz and avoid the vicinity of 60 Hz, where several strong peaks are present in the measured floor vibration spectra. Further analysis should be done once the girder mechanical design is more advanced and the resonant modes (frequencies, damping, and the modal structure) are available.

Future work should include simulation cross-checks for other lattices and operational energies (the results obtained so far are for the 2-IP lattice at 18 GeV only). We will also need to check the effects due to orbit or coupling bumps which are presently being studied to increase the vertical emittance to the

desired value. Furthermore, motions for longer time scales should be analyzed. In particular, the effects of the ground diffusion, commonly described by the ATL law (see e.g. [7]), will have implications for girder realignment frequency, required corrector strength, etc.

8. Acknowledgements

We are grateful to Mike Blaskiewicz and Christoph Montag as well as to Vadim Sajaev (APS) for the many insightful discussions and suggestions about this work.

9. References

[1] Electron-Ion Collider Conceptual Design Report, February, 2021, https://www.bnl.gov/ec/files/EIC_CDR_Final.pdf
[2] C. Montag et al., NIM-A, 564, 26–31, (2006), doi: 10.1016/j.nima.2006.03.030
[3] C. Montag et al., TPAP055, Proceedings of PAC05, Knoxville, Tennessee
[4] M. Borland, "elegant: A Flexible SDDS-Compliant Code for Accelerator Simulation," Advanced Photon Source LS-287, September 2000 gg
[5] MAD-X, http://mad.web.cern.ch.
[6] https://vibration.desy.de/
[7] A. Sery, O. Napoly, Phys.Rev. E 53, 5323, (1996).
[8] C. Spataro et al., https://doi.org/10.18429/JACoW-MEDSI2018-WEPH29
[9] N. Simos et al., SRN, Vol. 32, No. 5, 2019, https://doi.org/10.1080/08940886.2019.1654826
[10] K. Artoos et al., TH5RFP081, Proceedings of PAC09, Vancouver, BC, Canada
[11] V. Sajaev, C. Preissner, https://doi.org/10.18429/JACoW-IPAC2018-TUPMF012
[12] S. L. Miller and D. Childers, "Probability and Random Processes", Academic Press, 2nd edition, 2012